Sensors and Actuators B 244 (2017) 1016–1021

Contents lists available at ScienceDirect

Sensors and Actuators B: Chemical

journal homepage: www.elsevier.com/locate/snb

Sensing with ultra-short Fabry-Perot cavities written into optical micro-fibers

Stephen C. Warren-Smith [a,b,*], Ricardo M. André [a,c], Jan Dellith [a], Tina Eschrich [a], Martin Becker [a], Hartmut Bartelt [a]

[a] Leibniz Institute of Photonic Technology (IPHT Jena), Albert-Einstein-Straße 9, 07745 Jena, Germany
[b] Currently with School of Physical Sciences and Institute for Photonics and Advanced Sensing and ARC Centre of Excellence for Nanoscale BioPhotonics, The University of Adelaide, South Australia, 5005, Australia
[c] INESC TEC and Department of Physics and Astronomy, Faculty of Sciences, University of Porto, Rua do Campo Alegre 687, 4150-179 Porto, Portugal

ARTICLE INFO

Article history:
Received 8 September 2016
Received in revised form
29 November 2016
Accepted 11 January 2017
Available online 16 January 2017

Keywords:
Fabry-Perot
Optical fiber sensor
Optical fiber tapers
Focused ion beam

ABSTRACT

The small dimensions of optical fiber sensors are of particular interest to biological applications, given the ability to penetrate relatively inaccessible regions. However, conventional optical fibers are larger than biological material such as cells, and thus there is a need to further miniaturize fiber sensors. Here we present the fabrication of ultra-small Fabry-Perot cavities written into optical micro-fibers using focused ion beam milling. We have fabricated cavities as small as 2.8 μm and demonstrated their use for sensing of both bulk refractive index and thin-layer coatings. In order to achieve sensitive measurements we interrogate at visible wavelengths with a broadband detection system, thereby reducing the free spectral range of the interferometer relative to the measurement bandwidth, increasing the number of interference fringes, and allowing for the implementation of the Fourier shift method.

1. Introduction

Optical fiber sensors are of increasing interest in biological and biomedical applications, particularly for *in-vivo* applications where the fiber's small cross section can serve as a minimally invasive diagnostic instrument [1]. Physical sensing in biomedical and biomechanics applications, such as measuring temperature, pressure, and strain, is a relatively mature technology [2–4]. In order to extend beyond physical parameters and measure biochemical analytes a number of transduction strategies have been developed, which are usually categorized into either label-based detection (e.g. fluorescent tagging) or label-free through resonant or interferometric optical effects [5]. A commonly used label-free technique is surface plasmon resonance (SPR), which can be achieved by coating an optical fiber with a thinly coated metal such as silver or gold. Such devices are highly sensitive to the external environment, but it is difficult to create a multiplexed device due to the resonance being broadband and the high optical loss associated with metal coatings. SPR devices are also generally transmission devices, negating one of the useful advantages of optical fiber sensors, which is the ability to perform dip-sensing.

An alternative label-free transduction mechanism is to use interferometry, whereby changes in the optical path length of the interferometer, including the refractive index, are monitored [5,6]. Any of the traditional interferometric configurations can be implemented into the optical fiber, such as: Fabry-Perot; Michelson; Mach-Zehnder; and Sagnac interferometers [6]. While such sensors have been widely used for physical sensing, for label free refractive index sensing the challenge is to allow the propagating light to interact with the surrounding environment. For this reason Fabry-Perot interferometers are often used as either the cavity wall(s) can be coated with, or the cavity filled with, the analyte of interest [7–20]. Another advantage is the potential to perform either simultaneous measurement of multiple parameters (such as temperature and refractive index) [7–10,21] or multiplexed sensing [20,22–24] via multiple cavities.

A number of different techniques have been proposed for the fabrication of optical fiber Fabry-Perot sensors. Examples include femtosecond laser micro-machining [17,25,26], ultraviolet laser ablation [16], the use of wet etching and fusion splicing of single mode fibers [7,8], splicing etched single mode fiber to form a micro-gap [15], and splicing single-mode fiber to either capillary tubing [9,18], C-shaped fiber [19], or photonic crystal fiber [27]. A

* Corresponding author at: School of Physical Sciences and Institute for Photonics and Advanced Sensing and ARC Centre of Excellence for Nanoscale BioPhotonics, The University of Adelaide, South Australia, 5005, Australia.
E-mail address: stephen.warrensmith@adelaide.edu.au (S.C. Warren-Smith).

http://dx.doi.org/10.1016/j.snb.2017.01.081
0925-4005/

technique that can provide high surface quality and can be easily tailored for different cavity geometries is to use a focused-ion beam microscope to mill micro-cavities [10–14,28–31]. Milling the entire fiber cross section is possible, but is a highly time consuming process [10,29]. For this reason a number of different fiber geometries have been investigated in order to reduce the milling time such as: fiber tapers [11,13,31], polished fibers [12], etched fibers [14,28], and exposed-core microstructured optical fibers [30].

The focused ion beam milling technique is particularly suited to applications requiring very small spatial scales. Two particular examples were demonstrated by Kou et al., who milled cavities with lengths of 3.5 μm [13] and 4.4 μm [31] for refractive index and temperature sensing, respectively. However, in this case the cavity served as a reflective element in order to form a multi-mode interferometer within the optical fiber taper rather than as a true Fabry-Perot interferometer. One drawback from this scheme is that the device is less sensitive for refractive index sensing (110 nm/RIU) compared with true Fabry-Perot cavities, which, as explained below, are necessarily longer if measured in the C-band (e.g., 1067 nm/RIU for a 100 μm cavity [8], 1130 nm/RIU for a 25 μm cavity [16], and 1163 nm/RIU for a 60 μm cavity [17]), where RIU is refractive index units. Perhaps more significantly, the sensitivity of the multi-mode fiber-taper interferometer device is not restricted to only the cavity, but is sensitive along the entire tapered region with varying effect due to the evolution of the evanescent field along the taper. Thus the spatial resolution of this device is relatively large (millimeter scaled) and poorly defined.

A limitation in reducing the size of the cavity is that the free spectral range (FSR), in the wavelength domain, of the interference spectrum is inversely proportional to the cavity length (Eq. (1)),

$$FSR_\lambda = \frac{\lambda^2}{2nL} \quad (1)$$

where λ is the free space wavelength, L is the cavity length, and in the following analysis we neglect the effect of dispersion and thus n is the refractive index within the cavity. For example, a cavity with a length of 3.5 μm measured at infrared wavelengths (λ = 1.55 μm) will have a free spectral range of 340 nm, which is not possible to measure with the bandwidth of a typical infrared C-band erbium-based source. In order to measure clear Fabry-Perot fringes for such cavity lengths it is necessary to reduce the measurement wavelength and/or increase the measurement bandwidth.

In this work we demonstrate the ability to fabricate and analyze ultra-short Fabry-Perot cavities, down to 2.8 μm, in optical micro-fibers through the use of focused ion beam machining. By measuring at visible wavelengths with a broadband detection system these short cavity lengths still provide sufficient interference fringes to perform Fourier analysis. We analyze the bulk refractive index sensitivity at refractive indices relevant for sensing aqueous samples, and the surface coating sensitivity and biochemical sensing potential by depositing and measuring individual layers of polyelectrolyte coatings.

2. Methods

2.1. Sensor fabrication

To fabricate the sensor, first a standard single mode fiber (SMF28) was tapered using a filament fiber processing unit (Vytran GPX-3400). The approximate taper dimensions were: down-taper/waist/up-taper lengths of 10 mm each and a waist diameter of 10 μm. The taper was cleaved in half to form two micro-fiber tips, which were fixed at both ends onto an aluminum block using conductive glue. To reduce charging effects the sample was sputter coated with a 50 nm tantalum coating. As the tantalum coating can introduce loss through the evanescent field of the taper, a mask was used so that only the distal end of the taper, up to the point of the cavity writing, was coated.

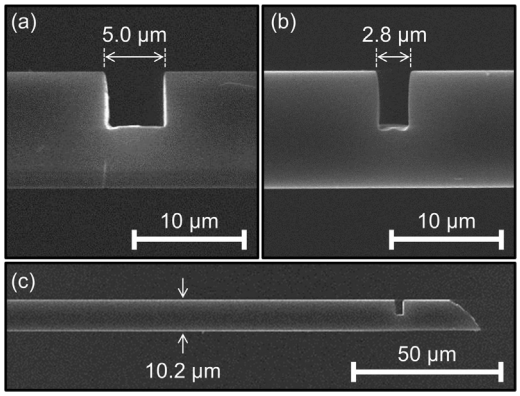

Fig. 1. Scanning electron microscope images of the Fabry-Perot optical micro-fiber cavities. (a) 5.0 μm cavity. (b) 2.8 μm cavity. (c) The 2.8 μm cavity, showing a section of the tapered micro-fiber including the angled tip to remove unwanted reflections.

Two different lengths of Fabry-Perot cavity were milled into the two micro-fiber tips using a Tescan (Lyra XMU) FIB-SEM (focused ion beam – scanning electron microscope). The cavities were milled using a polishing milling pattern with a current of 600 pA, first perpendicularly half-way into the taper, and then towards the left and right surfaces of the cavity to form the reflecting surfaces. The lengths of the two cavities were 5.0 μm (Fig. 1(a)) and 2.8 μm (Fig. 1(b)). The total milling time was less than 18 min for each cavity. The final step was to cleave the micro-fiber tip using the focused-ion beam at an angle of 45° in order to reduce unwanted reflections (Fig. 1(c)).

2.2. Optical measurements and the Fourier shift technique

The reflection spectra of the two cavities were measured using the setup shown in Fig. 2, which consisted of a super-continuum source (Fianium, WL-SC-400-2), a 25/75 fiber optic coupler (Thorlabs, TW560R3A1), and an optical spectrum analyzer (ANDO, AQ6315). The measured wavelength range was 460 nm–760 nm with a resolution of 1.0 nm. To obtain normalized reflection spectra the recorded spectra were compared against the reflection of a fiber optic retroreflector (Thorlabs).

For the sensing experiments each spectrum was analyzed with the Fourier shift method [32,33], whereby the phase of the interference pattern is extracted as the phase angle of the fast Fourier transform (FFT) peak. Silverstone et al. have previously demonstrated both experimentally and with numerical simulations that this technique is more sensitive than identifying shifts in the peak locations or curve fitting [33]. While this was in the context of whispering gallery modes, it can equally be applied to any interferometric signal given the periodicity of the spectrum. The benefit of this technique, particularly compared to peak tracking, can be

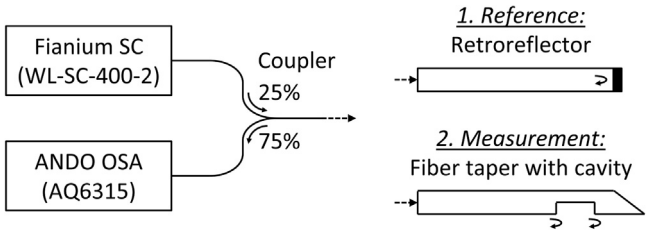

Fig. 2. Schematic diagram of the optical measurement setup. SC refers to supercontinuum, OSA refers to optical spectrum analyzer.

conceptually understood as resulting from making use of the full spectrum compared to just a small segment.

It is important to note that the Fourier shift method requires the fringe spacing (free spectral range) in the interference pattern to be uniform so that a single peak is formed in the fast Fourier transform power spectrum. However, neglecting dispersion, when measured relative to optical wavelength the free spectral range (Eq. (1)) is dependent on wavelength while the free spectral range measured relative to optical frequency is not (Eq. (2), c = speed of light constant).

$$FSR_\nu = \frac{c}{2nL} \tag{2}$$

Thus, for all sensing measurements the optical spectrum was first converted to optical frequency, using linear interpolation for even sampling, before applying the fast Fourier transform.

2.3. Sensing of bulk refractive index

The refractive index sensitivity of the cavities was measured by lowering the fiber tapers into a series of low concentration solutions of sodium chloride (NaCl). The solutions were prepared in steps of 0.002 refractive index units from n = 1.333 (water) to n = 1.345 (6.96 wt.% NaCl). The required concentrations were calculated by interpolating data in [34].

2.4. Sensing of polyelectrolyte layers

Polyelectrolyte solutions of 2 mg/ml poly(sodium styrene sulfonate) (PSS, Sigma-Aldrich, $M_w \approx 70{,}000$) and poly(allylamine hydrochloride) (PAH, Sigma-Aldrich, $M_w \approx 17{,}500$) in 1 M NaCl were prepared. Each cavity was then lowered alternatively into the PAH and PSS solutions for five minutes each. Between each step the cavity was immersed into water for five minutes for both rinsing and measurement of the optical reflection. Only measurements in the water rinsing step were considered in order to ensure that the bulk refractive index within the cavity was consistent and the resulting measurement was only from changes in the surface binding.

3. Results and discussion

3.1. Characterization of the cavity spectra

Typical reflection spectra for the cavity in air (green) and filled with water (purple) are shown in Fig. 3(a) for the 5.0 μm cavity and in Fig. 3(b) for the 2.8 μm cavity. As predicted by Eq. (1), there are a greater number of fringes for the longer cavity, with approximately 11 for the water-filled 5.0 μm cavity and six for the water-filled 2.8 μm cavity. Also observed overlapping the dominant spectrum is a short wavelength "noise" with a contrast of 1–2 dB. This is a result of the cavity formed between the milled cavity and the tip of the fiber, indicating that the 45° tip is not perfectly smooth. It is difficult to perform a polishing step on fiber tip using the focused ion beam microscope as the taper becomes free hanging when the cleave is made and vibrations due to the long length of the fiber prevent further machining to occur. In any case, an advantage of the Fourier shift method is that such noise can be effectively filtered and only shifts in the dominant fringes are tracked.

3.2. Sensing of bulk refractive index

As there is sufficient periodicity in the spectra shown in Fig. 3, it is possible to observe a clear peak in the fast Fourier transform power spectrum, as shown in Fig. 4(a). The phase angle of the fast Fourier transform at the position of this peak can then be used to

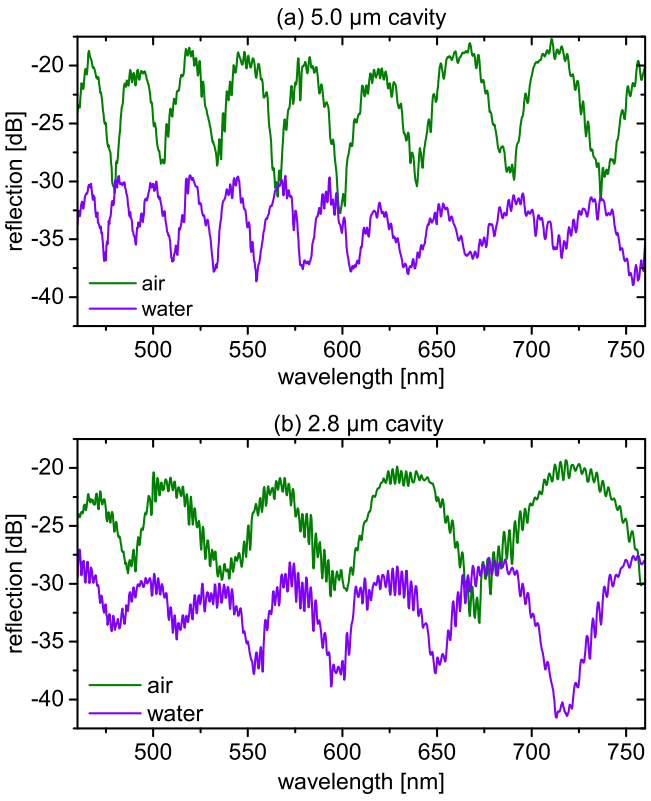

Fig. 3. Reflection spectra of the 5.0 μm cavity (a) and the 2.8 μm cavity (b), with the cavities containing either air (green) or water (purple). (For interpretation of the references to colour in this figure legend, the reader is referred to the web version of this article.)

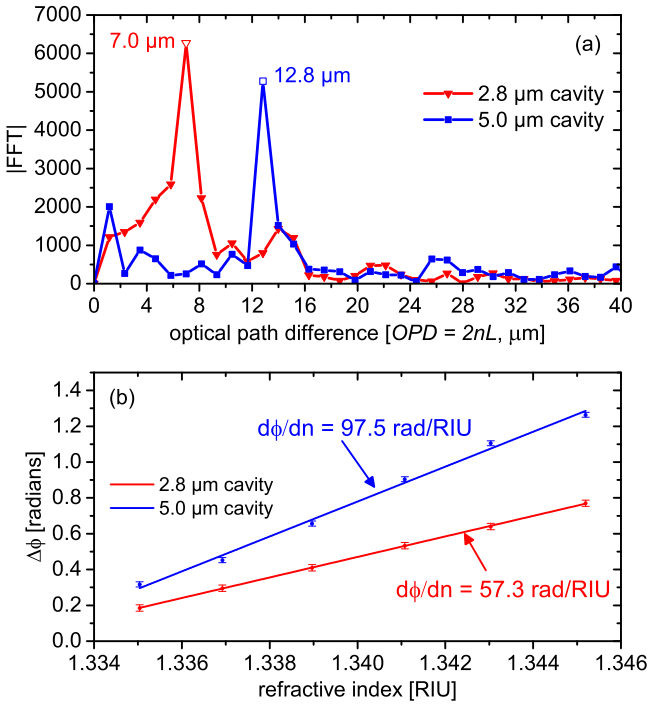

Fig. 4. (a) Fast Fourier transform (FFT) of the spectra in Fig. 2 when the cavities contain water (n = 1.333). The peak of the FFT is shown with open symbols. The phase angles associated with these points were used for sensing experiments. Note that the x-axis of the spectra in Fig. 2 was first converted to optical frequency using linear interpolation. (b) The refractive index sensitivity of the two cavities, in weak solutions of NaCl in water (range: 0–7 wt.%). Error bars indicate the 3σ variation over 60 consecutive measurements (approximately 1 h) when the cavities were filled with water.

extract sensitive information on shifts in the spectrum for sensing. This technique was applied to bulk refractive index sensing, where the phase shift in the interference spectrum relative to when the cavity is filled with water is shown in Fig. 4(b). The results show a highly linear response to refractive index within the range measured ($R^2 > 0.997$).

To understand the relative sensitivities of the two cavities, we first note that the Fabry-Perot cavity can be approximated as a two-wave interferometer given the reflectivity at each interface is small (≈3.5%) and thus multiple reflections are negligible. The resulting reflection spectrum, $I(\lambda)$, can then be represented as shown in Eq. (3),

$$I = I_1 + I_2 + 2\sqrt{I_1 I_2}\cos\left[\frac{2\pi}{\lambda}(2nL) + \pi\right], \quad (3)$$

where I_1 and I_2 are the reflected intensities from each cavity wall. Differentiating the cosine argument in Eq. (3) yields the sensitivity of the interference spectrum phase, &x3D5;, to refractive index (Eq. (4)).

$$\frac{\partial\phi}{\partial n} = \frac{4\pi L}{\lambda} \quad (4)$$

Taking the central wavelength of 610 nm, Eq. (4) gives an estimated sensitivity of 103 rad/RIU for the 5.0 μm cavity and 57.7 rad/RIU for the 2.8 μm cavity, which is within 6% of the experimental result. Measurements were also made to determine the minimum detection limit by recording the standard deviations over 60 measurements (approximately 1 h) while the cavities were immersed in water and multiplying by three to obtain the 3σ variation. This gives the 99.7% confidence level for a measurement on the time scale of one hour, and was determined to be ±0.014 rad for the 5.0 μm cavity and ±0.018 rad for the 2.8 μm cavity. This is a more practical limit than comparing the sensor sensitivity and optical spectrum analyzer resolution, which is difficult to achieve in practice due to noise. The measured 3σ variation implies single spectral scan detection limits of 2.9×10^{-4} RIU (5.0 μm cavity) and 6.3×10^{-4} RIU (2.8 μm cavity). By linearly extrapolating the phase sensitivity and noise for these two cavities it can be estimated that the minimum cavity length with a detection limit better than 10^{-3} RIU is 1.9 μm, which can be considered a practical limit for the particular conditions used here.

While the phase sensitivity and detection limit are the parameters of primary interest when using the Fourier shift method, for comparison Eq. (1) can be used to estimate a wavelength shift sensitivity of 407 nm/RIU (5.0 μm cavity) and 427 nm/RIU (2.8 μm cavity). This is close to the theoretical value of 457 nm/RIU, with the difference likely attributed to considering only the central wavelength (610 nm), rather than the full bandwidth used in the experiment.

3.3. Sensing of polyelectrolyte layer deposition

To add biochemical functionality to optical fiber sensors, one technique is to electrostatically bind alternating layers of positively and negatively charged polyelectrolytes to the glass surface [18,35]. The final coating layer can then be chosen to have appropriate functional groups, such as amine or carboxylic acid groups, for subsequent binding. As the electrostatic binding is a physical process, rather than chemical, this procedure can be applied to glass as well as other surfaces such as polymers [36] and metal coatings [37]. Polyelectrolyte coatings have the dual benefit that the coating procedure itself can be measured using interferometric techniques, including optical fiber Fabry-Perot interferometers [18]. The measured response can then be used as a calibration curve for subsequent biological binding. Here we have applied this technique to the ultra-short Fabry-Perot cavities in order to demonstrate the ability to perform measurements on the surface of the cavity walls.

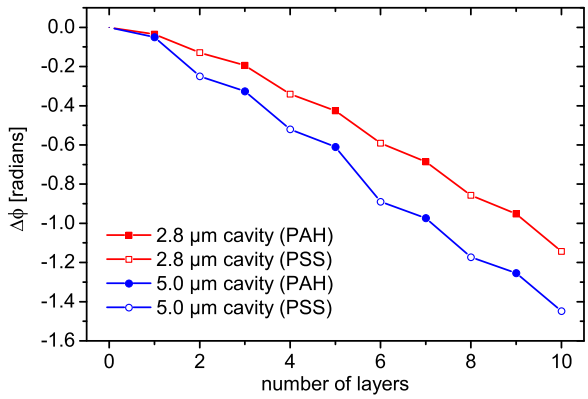

Fig. 5. Interference phase shift measured from the Fabry-Perot cavities for sequential coatings of positively charged (PAH, filled symbols) and negatively charged (PSS, open symbols) polyelectrolyte layers.

The Fourier shift method was applied and the results are shown in Fig. 5. It can be seen that there is a corresponding change in the interference phase with each coating layer. The shift is negative due to the polyelectrolyte coating, with a refractive index close to silica glass, effectively shortening the optical cavity length.

To estimate the corresponding layer thickness we can use Eq. (5), which is obtained by taking the derivative of the argument of the cosine function in Eq. (3) with respect to cavity length.

$$\frac{\partial\phi}{\partial L} = \frac{4\pi n}{\lambda} \quad (5)$$

We then make an approximation that the refractive index of the polyelectrolyte coatings is the same as the silica glass, thus the cavity is shortened by two times the coating thickness. This is not strictly accurate as the refractive index of polyelectrolyte layers is known to be the order of n = 1.54 [13], but we note that the polymer-air interface ($\Delta n \approx 0.21$) is dominant over the glass-polymer interface ($\Delta n \approx 0.09$) and thus the following calculations can be considered an order of magnitude check. Detailed analysis of the layer thickness could be achieved in future by including all four reflections, such as by implementing the transfer matrix method. Keeping this in mind, the average phase shift from the 5.0 μm cavity was measured to be 0.076 rad for the PAH layers and 0.21 rad for the PSS layers. This corresponds to thickness of 1.4 nm for the PAH layers and 3.9 nm for the PSS layers. This compares to 2.5 nm (PAH) and 4.5 nm (PSS) measured for a previously reported optical fiber Fabry-Perot sensor [18]. The difference may be attributed to factors such as the lower concentration used here (factor of two), the approximations made in the thickness calculation, differences in the polyelectrolyte molecular weight, phase noise in the interferometer, and the partially restricted geometry of the focused-ion beam milled cavity.

4. Discussion and conclusions

We have demonstrated the fabrication of ultra-small Fabry-Perot cavities in optical micro-fibers using focused-ion beam milling. The cavities fabricated were as short as 2.8 μm long, in 10 μm diameter tapered fibers. By interrogating at visible wavelengths with a broadband detection system the reflected interference pattern contains sufficient periodicity to analyze the changes in the optical path length of the cavity using the Fourier shift method. We have demonstrated these cavities for bulk refrac-

tive index sensing, with detection limits the order of 10^{-4} RIU, and for the detection of thin polymer coatings the order of 1 nm thick.

Future development of this sensor lies in adding biochemical functionality, such as via polyelectrolyte coatings. For example, specificity towards particular antigens can be achieved though the appropriate attachment of antibodies. There is also scope towards reducing the costs of, and miniaturizing, the detection system. The source and detector used in our work is based on optical communications characterization equipment, but improvements could be made by utilizing equipment designed for spectroscopy such as CCD (charged coupled device) linear array spectrometers. Such equipment is readily available, has high measurement speed, and is designed to operate at visible wavelengths.

Ultimately we believe such sensors will provide useful tools for the life sciences given these sensors can be made smaller than a cell. Intracellular measurements based on, for example, fluorescence [38,39] or surface enhanced Raman spectroscopy [40,41], have previously been demonstrated with optical fiber tapers. We envisage that our sensor will allow for new measurements of local physical and biochemical parameters within cells such as an individual oocyte (approximately 100 μm in diameter) for improving understanding in the process of fertilization, particularly in-vitro fertilization.

Acknowledgements

Stephen Warren-Smith is funded by the European Commission through the Seventh Framework Programme (FP7), PIIF-GA-2013-623248. Ricardo André is funded by Fundação para a Ciência e a Tecnologia (Portuguese Foundation for Science and Technology, UID/EEA/50014/2013 and SFRH/BD/84048/2012).

References

[1] X-d Wang, O.S. Wolfbeis, Fiber-optic chemical sensors and biosensors (2013–2015), Anal. Chem. 88 (2016) 203–227.
[2] E. Al-Fakih, N.A.A. Osman, F.R.M. Adikan, The use of fiber Bragg grating sensors in biomechanics and rehabilitation applications: the state-of-the-art and ongoing research topics, Sensors 12 (2012) 12890–12926.
[3] P. Roriz, L. Carvalho, O. Frazão, J.L. Santos, J.A. Simões, From conventional sensors to fibre optic sensors for strain and force measurements in biomechanics applications: a review, J. Biomech. 47 (2014) 1251–1261.
[4] P. Roriz, O. Frazão, A.B. Lobo-Ribeiro, J.L. Santos, J.A. Simões, Review of fiber-optic pressure sensors for biomedical and biomechanical applications, J. Biomed. Opt. 18 (2013) 050903.
[5] X.-D. Fan, I.M. White, S.I. Shopova, H.-Y. Zhu, J.D. Suter, Y.-Z. Sun, Sensitive optical biosensors for unlabeled targets: a review, Anal. Chim. Acta 620 (2008) 8–26.
[6] B.H. Lee, Y.H. Kim, K.S. Park, J.B. Eom, M.J. Kim, B.S. Rho, et al., Interferometric fiber optic sensors, Sensors 12 (2012) 2467–2486.
[7] Y. Zhang, X. Chen, Y. Wang, K.L. Cooper, A. Wang, Microgap multicavity Fabry-Perot biosensor, J. Lightwave Technol. 25 (2007) 1797–1804.
[8] S. Pevec, D. Donlagic, High resolution, all-fiber, micro-machined sensor for simultaneous measurement of refractive index and temperature, Opt. Express 22 (2014) 16241–16253.
[9] Y. Zhang, K.L. Cooper, A. Wang, Multicavity Fabry-Perot interferometric thin-film sensor with built-in temperature compensation, IEEE Photonic Tech. L 17 (2005) 2712–2714.
[10] L.V. Nguyen, M. Vasiliev, K. Alameh, Three-wave fiber Fabry-Pérot interferometer for simultaneous measurement of temperature and water salinity of seawater, IEEE Photonic Tech. L 23 (2011) 450–452.
[11] W. Yuan, F. Wang, A. Savenko, D.H. Peterson, O. Bang, Note: optical fiber milled by focused ion beam and its application for Fabry-Perot refractive index sensor, Rev. Sci. Instrum. 82 (2011) 076103.
[12] T. Wieduwilt, J. Dellith, F. Talkenberg, H. Bartelt, M.A. Schmidt, Reflectivity enhanced refractive index sensor based on a fiber-integrated Fabry-Perot microresonator, Opt. Express 22 (2014) 25333–25346.
[13] J.-L. Kou, J. Feng, Q.-J. Wang, F. Xu, Y.-Q. Lu, Microfiber-probe-based ultrasmall interferometric sensor, Opt. Lett. 35 (2010) 2308–2310.
[14] R.M. André, S.C. Warren-Smith, M. Becker, J. Dellith, M. Rothhardt, M.I. Zibaii, et al., Simultaneous measurement of temperature and refractive index using focused ion beam milled Fabry-Perot cavities in optical fiber micro-tips, Opt. Express 24 (2016) 14053–14065.
[15] Y. Wang, K.L. Cooper, A. Wang, Microgap structured optical sensor for fast label-free DNA detection, J. Lightwave Technol. 26 (2008) 3181–3185.
[16] Z. Ran, Y. Rao, J. Zhang, Z. Liu, B. Xu, A miniature fiber-optic refractive index sensor based on laser-machined Fabry-Perot interferometer tip, J. Lightwave Technol. 27 (2009) 5426–5429.
[17] T. Wei, Y. Han, Y. Li, H.-L. Tsai, H. Xiao, Temperature-insensitive miniaturized fiber inline Fabry-Perot interferometer for highly sensitive refractive index measurement, Opt. Express 16 (2008) 5764–5769.
[18] Y. Zhang, H. Shibru, K.L. Cooper, A. Wang, Miniature fiber-optic multicavity Fabry-Perot interferometric biosensor, Opt. Lett. 30 (2005) 1021–1023.
[19] C. Wu, Z. Liu, A.P. Zhang, B.-O. Guan, H.-Y. Tam, In-line open-cavity Fabry-Pérot interferometer formed by C-shaped fiber fortemperature-insensitive refractive index sensing, Opt. Express 22 (2014) 21757–21766.
[20] S.C. Warren-Smith, R.M. André, J. Dellith, H. Bartelt, Multiplexed refractive index-based sensing using optical fiber microcavities, Proc. SPIE 98991G (2016) (April 29, 2016).
[21] Y. Zhang, J. Huang, X. Lan, L. Yuan, H. Xiao, Simultaneous measurement of temperature and pressure with cascaded extrinsic Fabry-Perot interferometer and intrinsic Fabry-Perot interferometer sensors, Opt. Eng. 53 (2014) 067101.
[22] M. Singh, C.J. Tuck, G.F. Fernando, Multiplexed optical fibre Fabry-Perot sensors for strain metrology, Smart Mater. Struct. 8 (1999) 549–5453.
[23] Y.J. Rao, Recent progress in fiber-optic extrinsic Fabry-Perot interferometric sensors, Opt. Fiber Technol. 12 (2006) 227–237.
[24] J. Wang, B. Dong, E. Lally, J. Gong, M. Han, A. Wang, Multiplexed high temperature sensing with sapphire fiber air gap-based extrinsic Fabry-Perot interferometers, Opt. Lett. 35 (2010) 619–621.
[25] T. Wei, Y. Han, H.-L. Tsai, H. Xiao, Miniaturized fiber inline Fabry-Perot interferometer fabricated with a femtosecond laser, Opt. Lett. 33 (2008) 536–538.
[26] Y.-J. Rao, M. Deng, D.-W. Duan, X.-C. Yang, T. Zhu, G.-H. Cheng, Micro Fabry-Perot interferometers in silica fibers machined by femtosecond laser, Opt. Express 15 (2007) 14123–14128.
[27] Y.-J. Rao, M. Deng, D.-W. Duan, T. Zhu, In-line fiber Fabry-Perot refractive-index tip sensor based on endlessly photonic crystal fiber, Sens. Actuators A Phys. 148 (2008) 33–38.
[28] R.M. André, S. Pevec, M. Becker, J. Dellith, M. Rothhardt, M.B. Marques, et al., Focused ion beam post-processing of optical fiber Fabry-Perot cavities for sensing applications, Opt. Express 22 (2014) 13102–13108.
[29] X. Li, S. Lin, J. Liang, H. Oigawa, T. Ueda, High-sensitivity fiber-optic Fabry-Perot interferometer temperature sensor, Jpn. J. Appl. Phys. 51 (2012) 06FL10.
[30] S.C. Warren-Smith, R.M. André, C. Perrella, J. Dellith, H. Bartelt, Direct core structuring of microstructured optical fibers using focused ion beam milling, Opt. Express 24 (2016) 378–387.
[31] J-l. Kou, L. Feng, L. Ye, F. Xu, Y-q Lu, Miniaturized fiber taper reflective interferometer for high temperature measurement, Opt. Express 18 (2010) 14245–14250.
[32] S. Lane, P. West, A. François, A. Meldrum, Protein biosensing with fluorescent microcapillaries, Opt. Express 23 (2015) 2577–2590.
[33] J.W. Silverstone, S. McFarlane, C.P.K. Manchee, A. Meldrum, Ultimate resolution for refractometric sensing with whispering gallery mode microcavities, Opt. Express 20 (2012) 8284–8295.
[34] W.M. Haynes, CRC Handbook of Chemistry and Physics, CRC Press, 2014.
[35] L.V. Nguyen, K. Hill, S. Warren-Smith, T. Monro, Interferometric type optical biosensor based on exposed-core microstructured optical fiber, Sens. Actuators B Chem. 221 (2015) 320–327.
[36] T. Reynolds, A. François, N. Riesen, M.E. Turvey, S.J. Nicholls, P. Hoffmann, et al., Dynamic self-referencing approach to whispering gallery mode biosensing and its application to measurement within undiluted serum, Anal. Chem. 88 (2016) 4036–4040.
[37] A. François, J. Boehm, S.Y. Oh, T. Kok, T.M. Monro, Collection mode surface plasmon fibre sensors: a new biosensing platform, Biosens. Bioelectron. 26 (2010) 3154–3159.
[38] X.T. Zheng, C.M. Li, Single living cell detection of telomerase over-expression for cancer detection by an optical fiber nanobiosensor, Biosens. Bioelectron. 25 (2010) 1548–1552.
[39] T. Vo-Dinh, J.-P. Alarie, B.M. Cullum, G.D. Griffen, Antibody-based nanoprobe for measurement of a fluorescent analyte in a single cell, Nat. Biotechnol. 18 (2000) 764–767.
[40] T. Vo-Dinh, P. Kasili, M. Wabuyele, Nanoprobes and nanobiosensors for monitoring and imaging individual living cells, Nanomed. Nanotechnol. 2 (2006) 22–30.
[41] E.A. Vitol, Z. Orynbayeva, G. Friedman, Y. Gogotsi, Nanoprobes for intracellular and single cell surface-enhanced Raman spectroscopy (SERS), J. Raman Spectrosc. 43 (2012) 817–827.

Biographies

Stephen C. Warren-Smith completed his PhD in 2011 at the University of Adelaide, Australia, on the topic of microstructured optical fiber chemical sensing. He was then employed from 2011 to 2014 as an Australian Research Council (ARC) Super Science Fellow at the Institute for Photonics and Advanced Sensing and the School of Chemistry and Physics at the University of Adelaide, working on optical fiber biosensing for women's health applications. In 2015 and 2016 he worked as a European Union Marie Curie International Incoming Fellow at the Institute of Photonic

Technology, Jena, Germany, on a project investigating the micro/nano-structuring of optical fibers for sensing. Since October 2016 he is with the University of Adelaide as a Ramsay Fellow.

Jan Dellith was born 1973 in Jena, Germany. He studied material engineering at University of Applied Science Jena and received his PhD 2008 from the Bergakademie Freiberg. Since 2000 he works at IPHT Jena in particular in the field of solid state analytics.